

Calibrating the Dice loss to handle neural network overconfidence for biomedical image segmentation

Michael Yeung, Leonardo Rundo, Yang Nan, Evis Sala, Carola-Bibiane Schönlieb, Guang Yang

Abstract— The Dice similarity coefficient (DSC) is both a widely used metric and loss function for biomedical image segmentation due to its robustness to class imbalance. However, it is well known that the DSC loss is poorly calibrated, resulting in overconfident predictions that cannot be usefully interpreted in biomedical and clinical practice. Performance is often the only metric used to evaluate segmentations produced by deep neural networks, and calibration is often neglected. However, calibration is important for translation into biomedical and clinical practice, providing crucial contextual information to model predictions for interpretation by scientists and clinicians. In this study, we identify poor calibration as an emerging challenge of deep learning based biomedical image segmentation. We provide a simple yet effective extension of the DSC loss, named the DSC++ loss, that selectively modulates the penalty associated with overconfident, incorrect predictions. As a standalone loss function, the DSC++ loss achieves significantly improved calibration over the conventional DSC loss across five well-validated open-source biomedical imaging datasets. Similarly, we observe significantly improved when integrating the DSC++ loss into four DSC-based loss functions. Finally, we use softmax thresholding to illustrate that well calibrated outputs enable tailoring of precision-recall bias, an important post-processing technique to adapt the model predictions to suit the biomedical or clinical task. The DSC++ loss overcomes the major limitation of the DSC, providing a suitable loss function for training deep learning segmentation models for use in biomedical and clinical practice.

Index Terms— Biomedical Imaging, Image Segmentation, Machine Learning, Cost Function

This work was partially supported by The Mark Foundation for Cancer Research and Cancer Research UK Cambridge Centre [C9685/A25177], the CRUK National Cancer Imaging Translational Accelerator (NCITA) [C42780/A27066] and the Wellcome Trust Innovator Award, UK [215733/Z/19/Z]. This study was also partially supported by the British Heart Foundation (Project Number: TG/18/5/34111, PG/16/78/32402), the European Research Council Innovative Medicines Initiative (DRAGON, H2020-JTI-IMI2 101005122), the AI for Health Imaging Award (CHAIMELEON, H2020-SC1-FA-RTS-2019-1 952172), the UK Research and Innovation Future Leaders Fellowship (MR/V023799/1), and Imperial College UROP programme. Additional support was also provided by the National Institute of Health Research (NIHR) Cambridge Biomedical Research Centre [BRC-1215-20014] and the Cambridge Mathematics of Information in Healthcare (CMIH) [funded by the EPSRC grant EP/T017961/1]. The views expressed are those of the authors and not necessarily those of the NHS, the NIHR, or the Department of Health and Social Care. Corresponding authors: Michael Yeung and Guang Yang.

Michael Yeung is with the School of Clinical Medicine, University of Cambridge, Cambridge, UK. (e-mail: mjyy2@cam.ac.uk).

Michael Yeung, Leonardo Rundo and Evis Sala are with the Department of Radiology, University of Cambridge, Cambridge, UK.

Leonardo Rundo and Evis Sala are with the Cancer Research UK Cambridge Centre, University of Cambridge, Cambridge, UK. (e-mail: lr495@cam.ac.uk, es220@medsch.cam.ac.uk).

Leonardo Rundo is with the Department of Information and Electrical Engineering and Applied Mathematics (DIEM), University of Salerno, Italy

Carola-Bibiane Schönlieb is with the Department of Applied Mathematics and Theoretical Physics, University of Cambridge, Cambridge, UK. (e-mail: cbs31@cam.ac.uk).

Michael Yeung, Yang Nan and Guang Yang are with the National Heart & Lung Institute, Imperial College London, London, UK. (e-mail: y.nan20@imperial.ac.uk, g.yang@imperial.ac.uk).

I. INTRODUCTION

Image segmentation describes a per-pixel classification task, involving partitioning an image into semantic regions based on regional pixel characteristics [1]. However, class imbalance is frequently observed in biomedical image segmentation tasks, where objects, such as tumours or cell nuclei often occupy a small area relative to the background tissue [2]. This can hinder per-pixel classification accuracy and could result in poor segmentation results on biomedical images. To evaluate segmentation quality, the two most popular metrics used are the Dice similarity coefficient (DSC) and Jaccard index. Both metrics measure spatial overlap and are therefore generally robust to class imbalance [3], [4].

While the cross entropy (CE) loss is the most widely used loss function for classification, favoured because of its well calibrated prediction outputs, it is susceptible to class imbalance and regularly underperforms in these situations, particularly when very small segmentation targets are involved [5], [6]. In contrast, the DSC loss is, similar to its respective evaluation metric, robust to class imbalance and has been successfully applied to a variety of biomedical image segmentation tasks [7]–[9]. However, it is well known that optimising the DSC loss results in poorly calibrated, overconfident predictions (Figure 1) [10]–[12].

To incorporate automated image segmentation methods for biomedical applications, it is necessary that predictions are well calibrated, producing a distribution that matches the underlying uncertainty [11], [13], [14]. Even small differences in imaging hardware or image acquisition parameters may lead to a domain shift that could significantly affect neural network performance, and without proper calibration, result in overconfident predictions that could lead to false reassurance and possible harm [15]. Calibration also provides crucial contextual information to the corresponding segmentation output, which is useful for guiding clinical decision making, such as planning for surgical resection or image-guided interventions.

The dichotomy between the CE loss, which provides well calibrated but often suboptimal segmentations, and the DSC loss—which produces higher quality segmentations but results in poorly calibrated predictions—suggests that neither loss function is appropriate for clinical use.

To overcome these emerging challenges in biomedical image segmentation, considerable research has focused on either modifying the CE loss to improve robustness to class imbalance, or improving the calibration of networks trained using the DSC loss. The Focal loss is a variant of the CE loss that addresses the issue of class imbalance by down-weighting the contribution of easy examples enabling learning of harder examples [16]. Similarly, the exponentially weighted CE loss down-weights correctly predicted samples, but is better suited for smaller degrees of class imbalance [17]. In contrast to directly modifying the CE loss, approaches to improve DSC loss calibration generally focus on modifying the network or applying post hoc calibration. Performing dropout during inference, known as Monte Carlo (MC) dropout, was shown to approximate Bayesian neural networks and improve calibration [11], [14], [18]. Other network modifications where improved calibration was observed include Platt scaling, which involves fitting a logistic regression model using

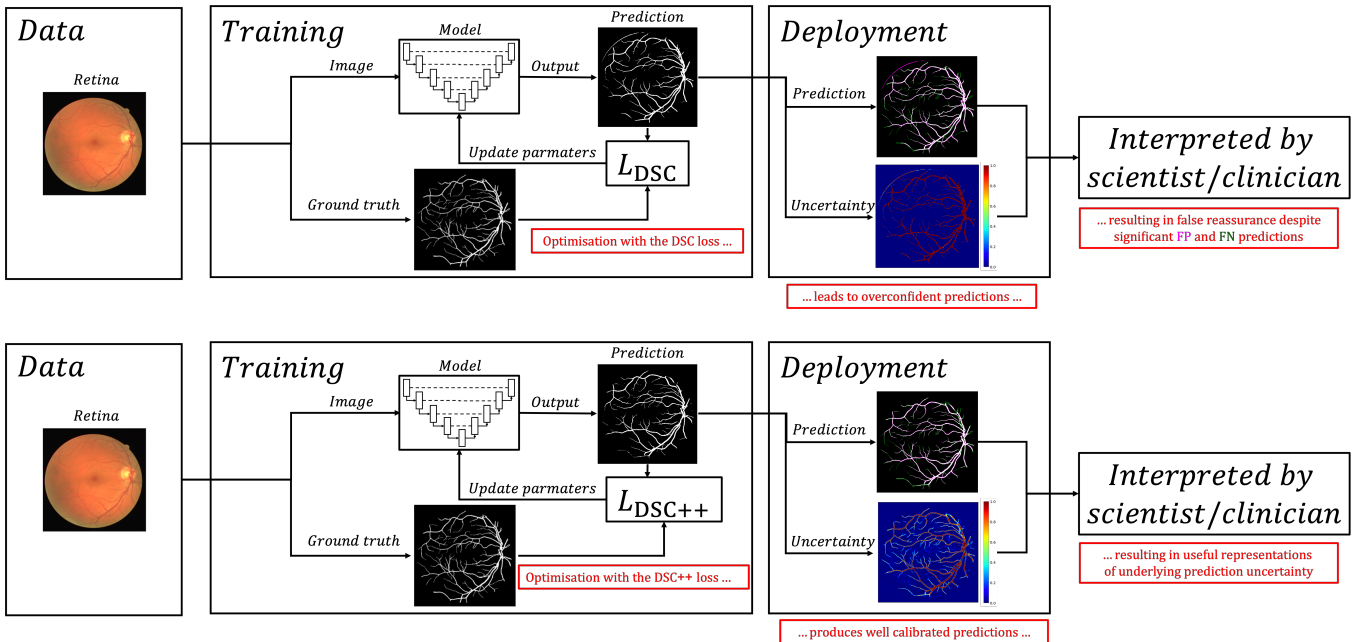


Fig. 1. Deep learning based biomedical image segmentation pipeline. During training, model predictions are compared to ground truth annotations, with model parameters iteratively updated based on the optimisation goal defined by the loss function. During deployment, the model is used for inference, generating a segmentation mask and associated softmax values, which are accessible by the scientist or clinician. Top: Using the DSC loss results in overconfident model predictions, demonstrated by the extreme softmax values illustrated by the heatmap, despite significant false positive (FP) and false negative (FN) predictions. Bottom: In contrast, using the DSC++ loss produces well calibrated predictions that, with a lower certainty, capture the more difficult-to-segment small-diameter retinal vessels. The colours corresponding to the softmax values are shown by the colour-bar on the right.

model outputs, as well as auxiliary networks, which are a generalised version of Platt scaling that instead uses a convolutional layer [19], [20]. Avoiding network modifications, deep ensembles involve averaging predictions from multiple, randomly initialised networks, outperforming MC dropout for both performance and calibration [11], [14], [21]. However, ensembling of multiple networks is not only computationally expensive to train, but significantly increases inference time and is therefore limited in real-world applications. Finally, improved calibration was observed by initially training a network using the DSC loss, followed by fine-tuning using the CE loss [14].

Despite various modifications to the CE loss, the segmentation performance remains generally worse than using the DSC loss [6]. In contrast, the modifications to improve the DSC loss calibration result in comparable calibration to the CE loss, but require pipeline modifications, limiting uptake by the research community as well as clinical applicability.

The main contributions of this work may be summarised as follows:

- 1) We identify the reason for the poor calibration observed with networks trained using the DSC loss, and provide a reformulation, named the DSC++ loss, which directly addresses the issue.
- 2) We demonstrate significantly improved calibration using the DSC++ loss over the DSC loss, measured using the negative log likelihood (NLL) and Brier scores, which is comparable to the calibration achieved using the CE loss, across five well-validated open-source datasets.
- 3) We demonstrate that the DSC++ loss may be readily incorporated to improve the calibration of other DSC-based loss functions.
- 4) We combine softmax thresholding with the DSC++ loss to

enable tailoring of the recall-precision bias for the biomedical or clinical task.

II. MATERIALS AND METHODS

In this section, we first introduce the CE loss, followed by the DSC loss. We then identify the cause of the poor calibration using the DSC loss, and use this to derive the DSC++ loss. After introducing softmax thresholding, the section finally concludes with details on the experiment setup and implementation.

A. CE loss

CE, denoted by $H(y, p)$, measures the difference between two probability distributions y and p . The CE loss is among the most widely used loss function in machine learning, and in the context of image segmentation, y and p represent the true and predicted distributions over class labels for a given pixel, respectively. The CE loss, (\mathcal{L}_{CE}), is defined as:

$$\mathcal{L}_{CE}(y, p) = -\frac{1}{N} \sum_{i=1}^N \sum_{c=1}^C y_{i,c} \cdot \log(p_{i,c}), \quad (1)$$

where $y_{i,c}$ uses a one-hot encoding scheme corresponding to the ground truth labels, $p_{i,c}$ is a matrix of predicted values generated by the model for each class, and where indices i and c iterate over all pixels and classes, respectively. The CE loss is a strictly proper scoring rule, superficially equivalent to the NLL, and therefore yields consistent probabilistic prediction [22].

B. DSC loss

CE is based on pixel-wise error, where in class imbalanced situations, using the CE loss results in over-representation of larger objects in the loss, and consequently under-segmentation of smaller

objects. Often the segmentation target in biomedical imaging tasks occupies a small area relative to the size of the image, limiting its use as a metric or loss function [6].

In contrast, the DSC is a spatial overlap index and therefore robust to class imbalance, and is defined as:

$$\text{DSC} = \frac{1}{C} \sum_{c=1}^C \frac{2 \sum_{i=1}^N p_{i,c} y_{i,c}}{\sum_{i=1}^N p_{i,c} + \sum_{i=1}^N y_{i,c}}, \quad (2)$$

where the DSC loss (\mathcal{L}_{DSC}) is:

$$\mathcal{L}_{\text{DSC}} = 1 - \text{DSC}. \quad (3)$$

C. DSC++ loss

The optimisation goal, for both the CE and the DSC loss, is for the neural network to produce confident, and correct, predictions matching the ground truth label. However, neural network overconfidence is a well known phenomenon associated with the DSC loss, but not with the CE loss. To understand this difference, we concentrate on the binary segmentation case and define two further, equivalent formulations of the \mathcal{L}_{DSC} (Eq. (3)), in terms of true positive (TP), false negative (FN) and false positive predictions (FP), as well as in terms of recall and precision:

$$\mathcal{L}_{\text{DSC}} = 1 - \frac{2\text{TP}}{2\text{TP} + \text{FP} + \text{FN}}, \quad (4)$$

and

$$\mathcal{L}_{\text{DSC}} = 1 - \frac{2(\text{Precision} \times \text{Recall})}{\text{Precision} + \text{Recall}}, \quad (5)$$

where,

$$\text{Recall} = \frac{\text{TP}}{\text{TP} + \text{FN}}, \quad (6)$$

$$\text{Precision} = \frac{\text{TP}}{\text{TP} + \text{FP}}. \quad (7)$$

When both classes are present in equal frequency, the error associated with the FP and FN predictions is not biased towards a particular class. However, in class imbalanced situations, high precision, low recall solutions are favoured, with over prediction of the dominant class [23]. Combined with an optimisation goal that favours confident predictions, this results in networks producing extremely confident, and often incorrect, predictions of the dominant class in regions of uncertainty.

To overcome this issue, we reformulate the DSC loss to more heavily penalise overconfident predictions. First, we define another equivalent formulation of the \mathcal{L}_{DSC} , identical in structure to Eq. (4):

$$\mathcal{L}_{\text{DSC}} = 1 - \frac{2 \sum_{i=1}^N p_{0i} y_{0i}}{2 \sum_{i=1}^N p_{0i} y_{0i} + \sum_{i=1}^N p_{0i} y_{1i} + \sum_{i=1}^N p_{1i} y_{0i}}, \quad (8)$$

where p_{0i} is the probability of pixel i belonging to the foreground, i.e. segmentation target and p_{1i} is the probability of pixel belonging to background class. Similarly, y_{0i} is 1 for foreground and 0 for background class, and conversely y_{1i} takes values of 1 for background and 0 for foreground class.

To penalise overconfidence for uncertain regions, we apply the focal parameter, γ , directly to the FP and FN predictions, defining the DSC++ loss ($\mathcal{L}_{\text{DSC}++}$):

$$\mathcal{L}_{\text{DSC}++} = 1 - \frac{2 \sum_{i=1}^N p_{0i} y_{0i}}{2 \sum_{i=1}^N p_{0i} y_{0i} + \sum_{i=1}^N (p_{0i} y_{1i})^\gamma + \sum_{i=1}^N (p_{1i} y_{0i})^\gamma}. \quad (9)$$

The DSC++ loss achieves selective penalisation of the overconfident predictions by transforming the penalty from a linear to an exponentially-weighted penalty. When $\gamma = 1$, the DSC++ loss is identical to the DSC loss. When $\gamma > 1$, overconfident predictions are more heavily penalised, with increasing values of γ resulting in successively larger penalties applied. Higher γ values therefore favour low confidence predictions. The optimal γ value must balance the maintenance of confident, correct predictions while suppressing confident but incorrect predictions.

D. Softmax thresholding

While the softmax function is not a proxy for uncertainty, the distribution of well calibrated softmax outputs are closely related to the underlying uncertainty, even for out-of-distribution data [24], [25]. To generate a class labelled segmentation output, the argmax function assigns each pixel with the class associated based on the highest softmax value. Rather than using the argmax function, we propose using a variable threshold that enables manual adjustment of model outputs to favour either precision or recall. Here, we define the output of a model using an indicator function, describing a per-pixel operation that compares the softmax output for the segmentation target, s , to a given softmax threshold \mathcal{T} :

$$I_s = \begin{cases} 1 & \text{if } s < \mathcal{T} \\ 0 & \text{otherwise} \end{cases}. \quad (10)$$

With this generalisation, the argmax function may be restated as a special case where $\mathcal{T} = 0.5$. Higher values of \mathcal{T} favour precision, while lower values favour recall.

E. Dataset descriptions and evaluation metrics

To evaluate our proposed loss function, we select five public, well-validated biomedical image segmentation datasets. For retinal vessel segmentation, we select the Digital Retinal Images for Vessel Extraction (DRIVE) dataset [26]. The DRIVE dataset consists of 40 coloured fundus photographs obtained from diabetic retinopathy screening in the Netherlands, with an image resolution of 768×584 pixels. The Breast UltraSound 2017 (BUS2017) dataset consists of 163 ultrasound images of breast lesions with an average image size of 760×570 pixels collected from the UDIAT Diagnostic Centre of the Parc Taulí Corporation, Sabadell, Spain [27]. Furthermore, we include the 2018 Data Science Bowl dataset, which contains 670 light microscopy images for nuclei segmentation [28]. For skin lesion segmentation, we use the ISIC2018: Skin Lesion Analysis Towards Melanoma Detection grand challenge dataset. This dataset contains 2,594 images of skin lesions with an average size of 2166×3188 pixels [29]. Finally, for colorectal polyp segmentation, we use the CVC-ClinicDB dataset, which consists of 612 frames containing polyps with image resolution 288×368 pixels, generated from 23 video sequences from 13 different patients using standard colonoscopy interventions with white light [30].

For all the experiments, except for the DRIVE dataset (which is already partitioned into 20 training and 20 test images), we randomly partitioned the other four datasets into 80% development and 20% test set. For all datasets, we partitioned the development set into 80% training set and 20% validation set. Except for the CVC-ClinicDB dataset (where the image resolution was retained), image resolutions are downsampled using bilinear interpolation. A summary of the datasets, image resolutions and data partitions are presented in Table 1.

To assess the loss functions, we select two evaluation metrics each for calibration and performance. For calibration, we use the NLL

TABLE I
SUMMARY OF THE DATASET DETAILS AND TRAINING SETUP USED IN THESE EXPERIMENTS.

Dataset	Segmentation	#Images	Image resolution	#Training	#Validation	#Test
DRIVE	Retinal vessel	40	512 x 512	16	4	20
BUS2017	Breast tumour	163	128 x 128	104	26	33
2018DSB	Cell nucleus	670	256 x 256	428	108	134
ISIC2018	Skin lesion	2596	512 x 512	1661	417	518
CVC-ClinicDB	Colorectal polyp	612	288 x 384	392	98	122

and Brier score, both strictly proper scoring rules. For both metrics, a lower score corresponds to better calibration. The NLL is equivalent to the CE loss in Eq. (1), while the Brier score (Brier) computes the mean squared error between predicted probability scores and the true class labels:

$$\text{Brier} = \frac{1}{C} \frac{1}{N} \sum_{i=1}^C \sum_{i=1}^N (y_i - p_i)^2. \quad (11)$$

For performance, we use the DSC as previously defined, and the Intersection over Union (IoU), also known as the Jaccard Index (Jaccard):

$$\text{Jaccard} = \frac{\text{TP}}{\text{TP} + \text{FP} + \text{FN}}. \quad (12)$$

Contrary to the calibration metrics, a higher DSC or Jaccard score corresponds to better performance.

F. Implementation details

For our experiments, we leveraged the Medical Image Segmentation with Convolutional Neural Networks (MIScnn) open-source Python library [31]. This is based on the Keras library using the Tensorflow backend, and all experiments were carried out using NVIDIA P100 GPUs.

Images were resized as described previously, and normalised to $[0, 1]$ using the z-score. We applied on-the-fly data augmentation with probability 0.15, including: scaling ($0.85 - 1.25 \times$), rotation (-15° to $+15^\circ$), mirroring (vertical and horizontal axes), elastic deformation ($\alpha \in [0, 900]$ and $\sigma \in [9.0, 13.0]$) and brightness ($0.5 - 2 \times$).

To investigate the effect of altering γ on the DSC++ loss, we perform a grid search, evaluating values $\gamma \in [0.5, 5]$.

To evaluate the loss functions, we trained the standard 2D UNet, with model parameters initialised using the Xavier initialisation [32]. We trained each model with instance normalisation, using the stochastic gradient descent optimiser with a batch size of 1 and initial learning rate of 0.1 [33]. For convergence criteria, we used ReduceLROnPlateau to reduce the learning rate by 0.1 if the validation loss did not improve after 25 epochs, and the EarlyStopping callback to terminate training if the validation loss did not improve after 50 epochs.

To evaluate the effect of substituting the DSC loss for the DSC++ loss in several DSC-based variants commonly used to achieve state-of-the-art results, we selected the Tversky loss, Focal Tversky loss, Combo loss and Unified Focal loss [6], [23], [34], [35]. The Combo loss ($\mathcal{L}_{\text{Combo}}$) is a compound loss function defined as the weighted sum of the DSC and modified CE loss (\mathcal{L}_{mCE}) [35]:

$$\mathcal{L}_{\text{Combo}} = \alpha (\mathcal{L}_{\text{mCE}}) - (1 - \alpha) \cdot \text{DSC}, \quad (13)$$

where:

$$\mathcal{L}_{\text{mCE}} = -\frac{1}{N} \sum_{i=1}^N \beta (y_i \log(p_i)) + (1 - \beta) [(1 - y_i) \ln(1 - p_i)]; \quad (14)$$

the parameters α and β take values in the range $[0, 1]$, controlling the relative contribution of the DSC and CE terms to the loss, and the relative weights assigned to false positives and negatives, respectively. Optimising models with the Combo loss has been observed to improve performance, as well as produce visually more consistent segmentations over models trained using the component losses [36].

To overcome the high precision, low recall bias associated with the DSC loss, the Tversky loss ($\mathcal{L}_{\text{Tversky}}$) modifies the weights associated with the FP and FN predictions [23]:

$$\mathcal{L}_{\text{Tversky}} = 1 - \text{TI}, \quad (15)$$

where the Tversky index (TI) is defined as:

$$\text{TI} = \frac{\sum_{i=1}^N p_{0i}g_{0i}}{\sum_{i=1}^N p_{0i}g_{0i} + \alpha \sum_{i=1}^N p_{0i}g_{1i} + \beta \sum_{i=1}^N p_{1i}g_{0i}}, \quad (16)$$

where α and β control the FP and FN weightings, respectively.

To handle class imbalanced data, the Focal Tversky loss (\mathcal{L}_{FT}) applies a focal parameter γ to alter the weights associated with difficult to classify examples [34]:

$$\mathcal{L}_{\text{FT}} = \sum_{c=1}^C (1 - \text{TI})^{\frac{1}{\gamma}}, \quad (17)$$

$\gamma < 1$ increases the degree of focusing on harder examples.

Finally, the Unified Focal loss (\mathcal{L}_{UF}) generalises distribution-based and region-based loss functions into a single framework [6], and is defined as the weighted sum of the Asymmetric Focal loss (\mathcal{L}_{AF}) and Asymmetric Focal Tversky loss (\mathcal{L}_{AFT}):

$$\mathcal{L}_{\text{UF}} = \lambda \mathcal{L}_{\text{AF}} + (1 - \lambda) \mathcal{L}_{\text{AFT}}, \quad (18)$$

where:

$$\mathcal{L}_{\text{AF}} = -\frac{\delta}{N} y_{i:r} \log(p_{t,r}) - \frac{1 - \delta}{N} \sum_{c \neq r} (1 - p_{t,c})^\gamma \log(p_{t,r}), \quad (19)$$

$$\mathcal{L}_{\text{AFT}} = \sum_{c \neq r} (1 - \text{TI}) + \sum_{c=r} (1 - \text{TI})^{1-\gamma}, \quad (20)$$

where the TI is redefined as:

$$\text{TI} = \frac{\sum_{i=1}^N p_{0i}g_{0i}}{\sum_{i=1}^N p_{0i}g_{0i} + \delta \sum_{i=1}^N p_{0i}g_{1i} + (1 - \delta) \sum_{i=1}^N p_{1i}g_{0i}}. \quad (21)$$

The three hyperparameters are λ , which controls the relative weights of the two component losses, δ , which controls the relative weighting of positive and negative examples, and γ , which controls the relative weighting of easy and difficult examples.

We used the optimal hyperparameters as described in the original papers, detailed in Table 2. For each loss function, we substituted the DSC component of the loss for the DSC++ loss, setting $\gamma = 2$.

To test for statistical significance, we used the Wilcoxon rank sum test. A statistically significant difference was defined as $p < 0.05$.

To evaluate effect of softmax thresholding, we selected thresholds $\mathcal{T} \in [0.05, 0.95]$ using the DSC and DSC++ loss on the DRIVE dataset. The source code is available at <https://github.com/mlyg/DicePlusPlus>.

TABLE II

HYPERPARAMETER SETTINGS USED IN THESE EXPERIMENTS FOR THE DSC AND CROSS-ENTROPY BASED VARIANT LOSS FUNCTIONS.

Loss	Hyperparameter				
	α	β	γ	δ	λ
Tversky	0.3	0.7	-	-	-
Focal Tversky	0.3	0.7	$\frac{4}{3}$	-	-
Combo	0.5	0.5	-	-	-
Unified Focal	-	-	0.1	0.6	0.5

III. RESULTS

In this section, we first describe the results for the hyperparameter experiments using the DSC++ loss, before comparing the DSC loss, CE loss and DSC++ loss on the five biomedical imaging datasets. Next, we compare the effects of softmax thresholding using the DSC and DSC++ loss on recall-precision bias. Finally, we compare the performance and calibration of various DSC-based loss functions with and without the DSC++ modification.

A. DSC++ loss hyperparameter tuning

The results for the hyperparameter experiments using the DSC++ loss are shown in Table 2.

Most noticeable is the significant decrease in the NLL with values of $\gamma > 1$. The NLL decreases with increasing gamma, appearing to plateau at $\gamma = 0.2$. Similarly, Brier score decreases with increasing γ , with the lowest Brier scores at γ values of 0.2 and 0.25. With $\gamma = 0.2$, there is a statistically significance difference in NLL ($p = 6 \times 10^{-8}$) and Brier ($p = 2 \times 10^{-7}$) scores compared to the DSC loss. However, above this range, increasing gamma leads to an increase in Brier score. In terms of performance metrics, the highest DSC and Jaccard scores were observed with $\gamma = 0.2$, at 0.808 and 0.678 respectively. There is no statistically significant difference between the DSC and Jaccard scores using different γ values, suggesting that the improved calibration score does not come at the cost to performance.

To understand whether γ improves calibration scores by reducing model overconfidence, Figure 2 shows an example of the softmax probability outputs for an example test-set image.

With increasing γ values, there is a reduction in overconfident model predictions, in comparison to the DSC loss ($\gamma = 1$), where model predictions are concentrated at the extremes. Importantly, the low confidence areas are concentrated around the difficult to segment smaller retinal vessels, providing an plausible approximation of the underlying uncertainty.

B. Loss function comparisons

The DSC loss, CE loss and DSC++ loss were evaluated on five biomedical imaging datasets. Based on the results from the hyperparameter investigation, we set $\gamma = 2$ for the DSC++ loss. The results are shown in Table 3.

Firstly, there was a statistically significant difference between the NLL using DSC++ loss compared to the DSC loss, across all datasets (DRIVE: $p = 6 \times 10^{-8}$, BUS2017: $p = 0.01$, 2018DSB: $p = 8 \times 10^{-13}$, ISIC2018: $p = 1 \times 10^{-12}$ and CVC-ClinicDB: $p = 2 \times 10^{-11}$). There was no significant difference between the NLL values using the CE or DSC++ loss. The DSC++ loss achieved

the lowest Brier score for all five datasets, with statistically significant differences observed on the DRIVE ($p = 2 \times 10^{-7}$), ISIC2018 ($p = 0.01$) and CVC-ClinicDB ($p = 0.04$) datasets compared to the DSC loss. The DSC++ loss achieved the highest DSC score for four out of the five datasets, and the highest Jaccard score for three out of the five datasets. In contrast, the CE loss achieved the lowest DSC and Jaccard scores for four out of the five datasets. A statistically significant difference ($p < 0.05$) was observed on the DRIVE dataset for both the DSC and Jaccard scores between the DSC++ and CE loss.

Example segmentations using each loss function for the five datasets are shown in Figure 3. Visually, the best segmentations are observed using the DSC++ loss. In contrast, the DSC loss, despite very confident predictions, produces considerable false positive predictions such as in the BUS2017 example, as well as false negative predictions as seen in the CVC-ClinicDB example.

C. Incorporating the DSC++ loss into other Dice-based loss functions

The DSC loss forms the basis for several other region-based loss functions, and therefore we investigate the effect of instead incorporating the DSC++ loss modification. The results are shown in Table 4.

The DSC-based variants appear to all inherit the poorly calibrated nature of the DSC loss, except for the two compound loss functions, the Combo loss and the Unified Focal loss, that also incorporate the CE-based variants. However, using the DSC++ loss led to significant improvements in calibration for all loss functions compared, for both the NLL and Brier scores. Similarly, the highest performance, measured using the DSC and Jaccard scores, were obtained using the DSC++ variants.

D. Softmax thresholding

The effect of softmax thresholding on the performance of the DSC and DSC++ loss for the DRIVE dataset are shown in Figure 4. The DSC loss predictions display almost no variation across the entire range of softmax thresholds. In contrast, there are significant variations in recall and precision scores using the DSC++ loss. Importantly, considerable increases in recall or precision between $\mathcal{T} = 0.3$ and $\mathcal{T} = 0.7$ did not affect the DSC score. The DSC++ loss may be also tailored to provide very high recall or precision values, with little effect on the DSC score, achieving 0.923 precision and 0.748 DSC at $\mathcal{T} = 0.8$, and 0.923 recall and 0.761 DSC at $\mathcal{T} = 0.2$.

IV. DISCUSSION

In this work, we identified the weights associated with the FP and FN predictions as the reason for the poor calibration associated with the DSC loss, and used this to provide a reformulation, known as the DSC++ loss, which uses a γ parameter to more heavily penalise overconfident predictions. We observed significantly improved calibration using the DSC++ loss over the DSC loss, measured using the NLL and Brier scores, across five well-validated open-source datasets. Furthermore, we demonstrated that the variants of the DSC loss inherit poor calibration, while those using DSC++ variants led to significant improvements in calibration. Finally, we evaluated the effect of softmax thresholding on the DSC loss and DSC++ loss, where little variation in recall or precision was observed with the DSC loss, in comparison to the significant variation achievable using the DSC++ loss.

Modifying the loss function, rather than the network or training setup, is the most intuitive solution to improve calibration. This is

TABLE III

CALIBRATION AND PERFORMANCE OF THE DSC++ LOSS ON THE DRIVE DATASET WITH DIFFERENT γ VALUES. THE 95% CONFIDENCE INTERVALS ARE SHOWN IN BRACKETS. THE HIGHEST SCORES ARE DENOTED IN BOLD.

Gamma	Uncertainty		Performance	
	NLL (\downarrow)	Brier (\downarrow)	Dice (\uparrow)	Jaccard (\uparrow)
0.5	0.281 (0.244-0.318)	0.033 (0.032-0.034)	0.804 (0.798-0.810)	0.673 (0.665-0.681)
1.0	0.204 (0.177-0.231)	0.031 (0.030-0.032)	0.804 (0.797-0.811)	0.672 (0.662-0.682)
1.5	0.067 (0.057-0.077)	0.026 (0.025-0.027)	0.804 (0.797-0.811)	0.673 (0.663-0.683)
2.0	0.041 (0.035-0.047)	0.024 (0.023-0.025)	0.808 (0.802-0.814)	0.678 (0.670-0.686)
2.5	0.038 (0.033-0.043)	0.024 (0.023-0.025)	0.804 (0.797-0.811)	0.673 (0.663-0.683)
3.0	0.038 (0.034-0.042)	0.027 (0.026-0.028)	0.797 (0.789-0.805)	0.664 (0.653-0.675)
3.5	0.035 (0.031-0.039)	0.031 (0.030-0.032)	0.804 (0.797-0.811)	0.672 (0.662-0.682)
4.0	0.038 (0.035-0.041)	0.034 (0.033-0.035)	0.796 (0.788-0.804)	0.661 (0.650-0.672)
4.5	0.039 (0.036-0.042)	0.042 (0.041-0.043)	0.795 (0.787-0.803)	0.660 (0.649-0.671)
5.0	0.041 (0.038-0.044)	0.048 (0.047-0.049)	0.794 (0.786-0.802)	0.658 (0.647-0.669)

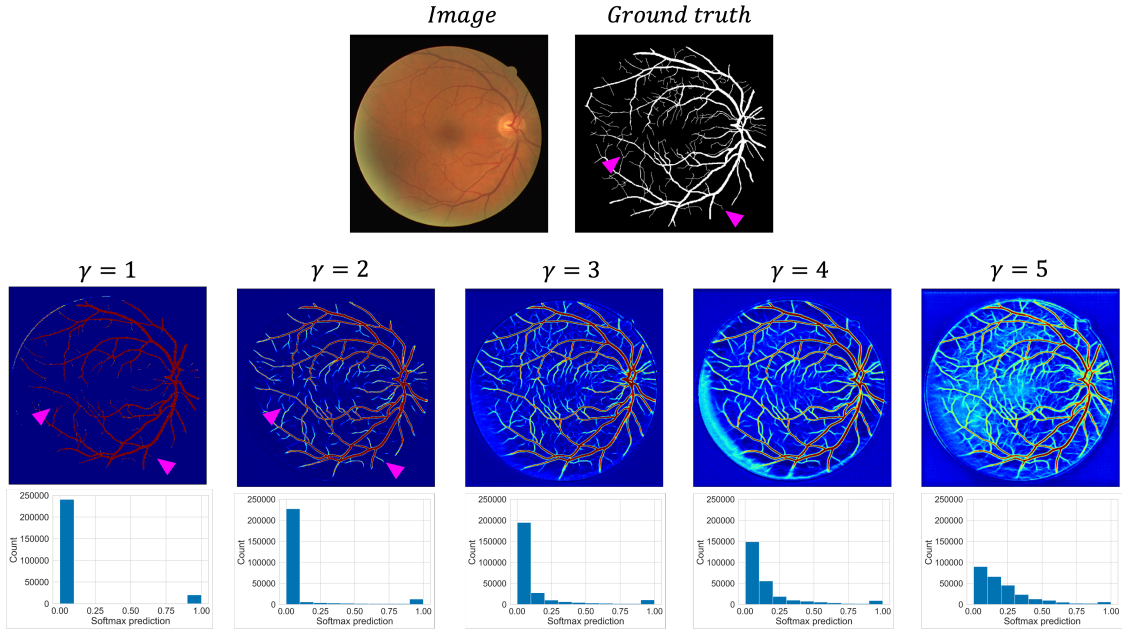


Fig. 2. The effect of altering γ on the softmax prediction outputs. Top: input image and ground truth segmentation. The pink arrows highlight example areas where segmentation quality differs. Middle: the softmax predictions for each model trained using the DSC++ loss with different γ value are displayed as heatmaps. Bottom: Histogram plots showing the softmax predictions and corresponding number of pixels.

TABLE IV

CALIBRATION AND PERFORMANCE OF DIFFERENT LOSS FUNCTIONS ON FIVE BIOMEDICAL IMAGING DATASETS. THE 95% CONFIDENCE INTERVALS ARE SHOWN IN BRACKETS. THE HIGHEST SCORES ARE DENOTED IN BOLD.

Dataset	Loss	Calibration		Performance	
		NLL (\downarrow)	Brier (\downarrow)	Dice (\uparrow)	Jaccard (\uparrow)
DRIVE	DSC	0.204 (0.177-0.231)	0.031 (0.030-0.032)	0.804 (0.797-0.811)	0.672 (0.662-0.682)
	CE	0.051 (0.045-0.057)	0.024 (0.023-0.025)	0.798 (0.790-0.806)	0.664 (0.653-0.675)
	DSC++	0.041 (0.035-0.047)	0.024 (0.023-0.025)	0.808 (0.802-0.814)	0.678 (0.670-0.686)
BUS2017	DSC	0.137 (0.044-0.230)	0.022 (0.013-0.031)	0.784 (0.708-0.860)	0.688 (0.603-0.773)
	CE	0.020 (0.011-0.029)	0.014 (0.008-0.020)	0.787 (0.713-0.861)	0.690 (0.608-0.772)
	DSC++	0.034 (0.001-0.067)	0.013 (0.006-0.020)	0.842 (0.780-0.904)	0.756 (0.688-0.824)
2018DSB	DSC	0.167 (0.129-0.205)	0.025 (0.021-0.029)	0.916 (0.905-0.927)	0.852 (0.835-0.869)
	CE	0.033 (0.026-0.040)	0.019 (0.016-0.022)	0.912 (0.900-0.924)	0.845 (0.827-0.863)
	DSC++	0.033 (0.026-0.040)	0.019 (0.016-0.022)	0.916 (0.905-0.927)	0.850 (0.833-0.867)
ISIC2018	DSC	0.373 (0.300-0.446)	0.044 (0.037-0.051)	0.883 (0.871-0.895)	0.812 (0.797-0.827)
	CE	0.083 (0.064-0.102)	0.036 (0.030-0.042)	0.863 (0.848-0.878)	0.787 (0.770-0.804)
	DSC++	0.086 (0.064-0.108)	0.034 (0.029-0.039)	0.882 (0.870-0.894)	0.811 (0.796-0.826)
CVC-ClinicDB	DSC	0.167 (0.101-0.233)	0.019 (0.014-0.024)	0.884 (0.857-0.911)	0.817 (0.785-0.849)
	CE	0.041 (0.025-0.057)	0.015 (0.011-0.019)	0.870 (0.842-0.898)	0.796 (0.763-0.829)
	DSC++	0.037 (0.023-0.051)	0.013 (0.010-0.016)	0.894 (0.864-0.924)	0.829 (0.799-0.859)

because with optimal training, it is the loss function that primarily determines the calibration quality of the resulting segmentation outputs. Optimisation with the DSC loss will encourage overconfident

predictions (Figure 1), and therefore methods—such as MC dropout or deep ensembling—may improve calibration, but do not address the direct cause of the issue. Importantly, both MC dropout and deep

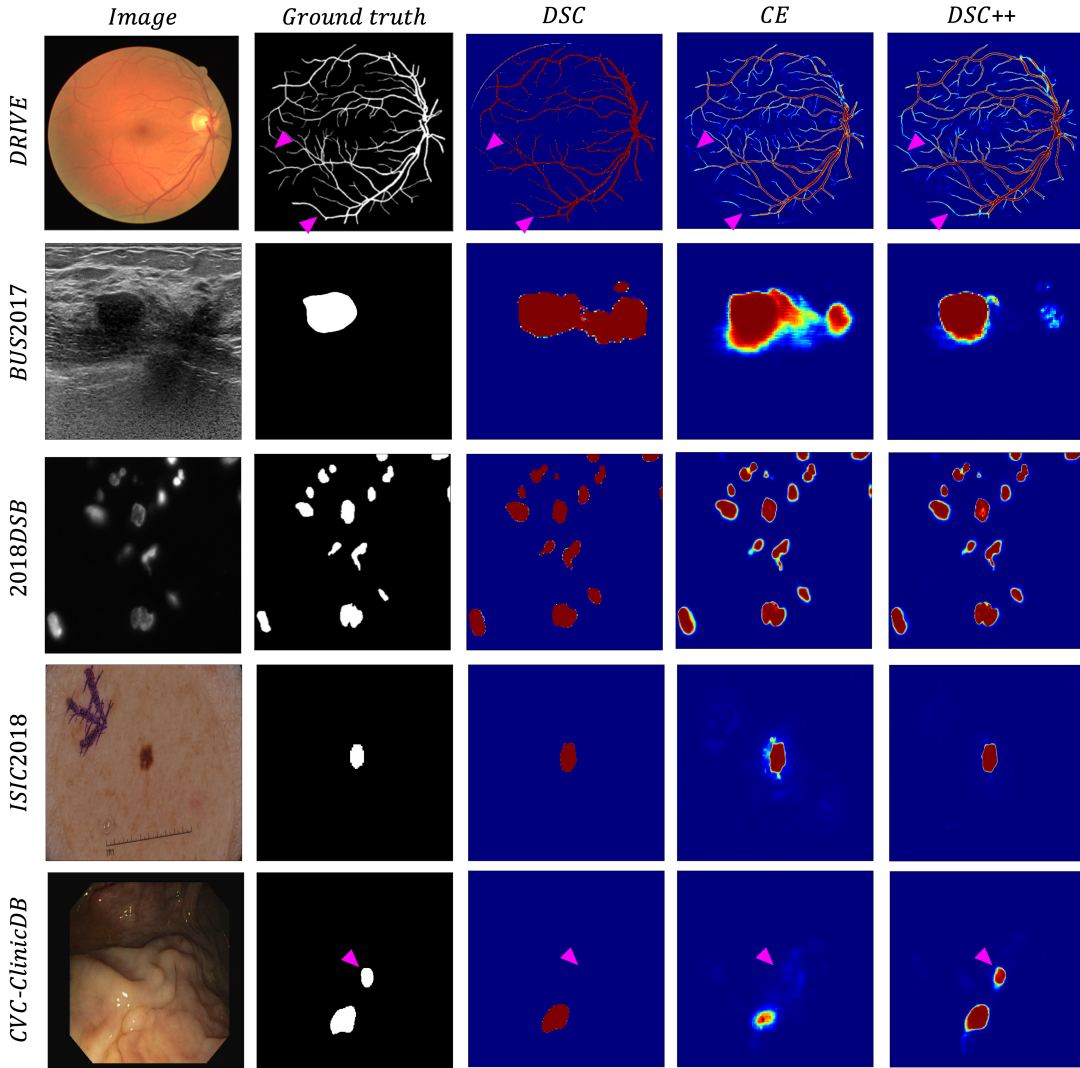


Fig. 3. Example segmentations, with softmax predictions visualised as a heatmap, for each loss function for each of the five datasets. The image and ground truth are provided for reference. The pink arrows highlight example areas where segmentation quality differs.

TABLE V

CALIBRATION AND PERFORMANCE OF THE DSC-BASED LOSS FUNCTIONS, USING EITHER THE ORIGINAL LOSS FUNCTIONS (TVERSKY, FOCAL TVERSKY, COMBO AND UNIFIED FOCAL) OR SUBSTITUTING THE DSC COMPONENT OF THE LOSS FOR THE DSC++ LOSS (TVERSKY++, FOCAL TVERSKY++, COMBO++ AND UNIFIED FOCAL++) LOSS. γ IS SET TO 2 FOR THE DSC++ VARIANTS. THE 95% CONFIDENCE INTERVALS ARE SHOWN IN BRACKETS. THE HIGHEST SCORES ARE DENOTED IN BOLD.

Loss	Calibration		Performance	
	NLL (\downarrow)	Brier (\downarrow)	Dice (\uparrow)	Jaccard (\uparrow)
Tversky	0.144 (0.121-0.167)	0.034 (0.033-0.035)	0.807 (0.802-0.812)	0.676 (0.668-0.684)
Tversky++	0.033 (0.028-0.038)	0.025 (0.024-0.026)	0.810 (0.804-0.816)	0.681 (0.673-0.689)
Focal Tversky	0.142 (0.120-0.164)	0.033 (0.032-0.034)	0.807 (0.802-0.812)	0.677 (0.670-0.684)
Focal Tversky++	0.036 (0.031-0.041)	0.024 (0.023-0.025)	0.810 (0.805-0.815)	0.680 (0.672-0.688)
Combo	0.063 (0.054-0.072)	0.025 (0.024-0.026)	0.802 (0.795-0.809)	0.669 (0.659-0.679)
Combo++	0.050 (0.043-0.057)	0.024 (0.023-0.025)	0.802 (0.795-0.809)	0.670 (0.661-0.679)
Unified Focal	0.056 (0.047-0.065)	0.026 (0.025-0.027)	0.810 (0.804-0.816)	0.680 (0.672-0.688)
Unified Focal++	0.039 (0.034-0.044)	0.024 (0.023-0.025)	0.810 (0.804-0.816)	0.681 (0.673-0.689)

ensembling significant increase inference time, with the second one further requiring additional computational resources to handle predictions from multiple networks. Furthermore, MC dropout requires modifying networks to include dropout layers, and this may not be compatible with certain architectures.

We also explored the synergistic effect of softmax thresholding, together with well calibrated outputs, to enable tailoring towards

high recall or high precision output states (Figure 4). For biomedical or clinical use, generally high recall is favoured, especially when the role of the automatic segmentation systems is to support human operators in reducing false negative predictions, for example with polyp identification during colonoscopy [37]. As shown in Figure 4, it is possible to identify even the small diameter retinal vessels when recall is prioritised. It is possible to optimise models to produce high

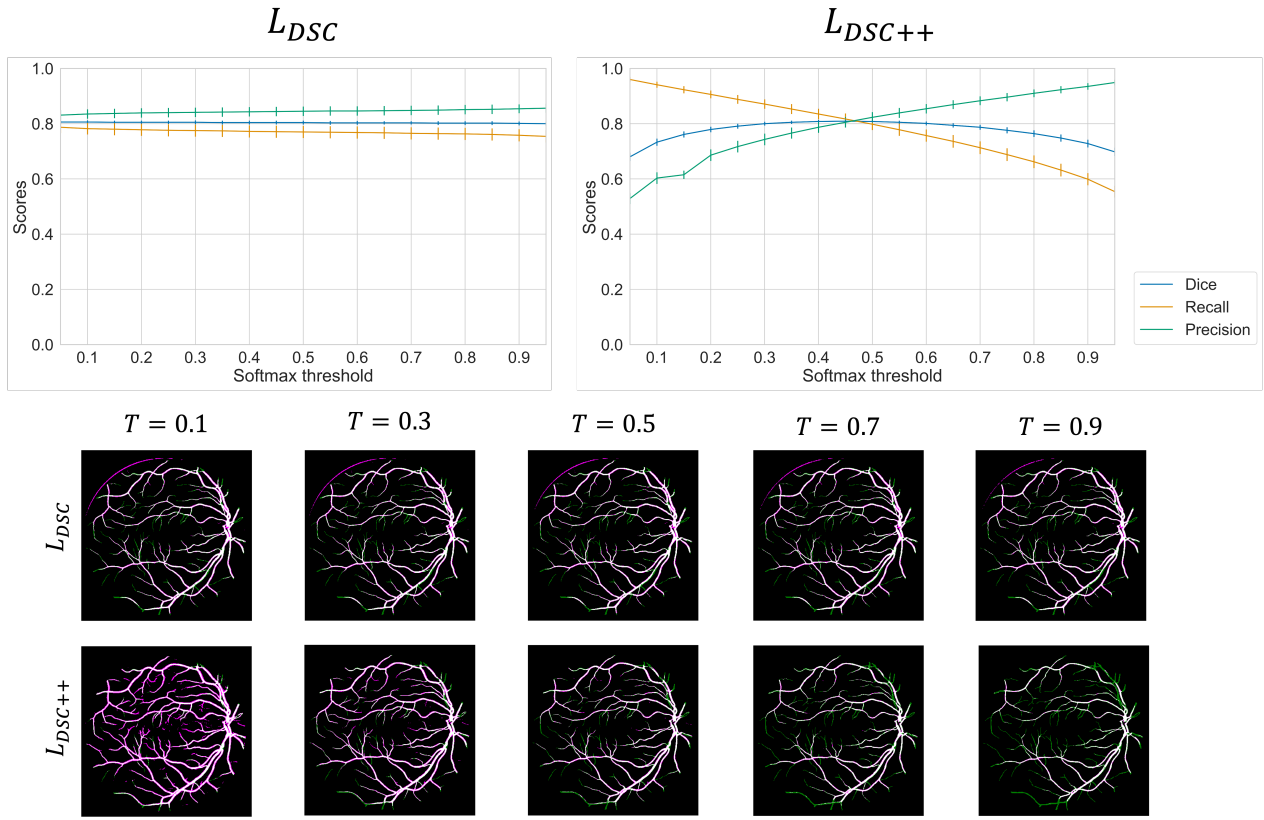


Fig. 4. The effect of softmax thresholding on the recall and precision using models trained with the DSC and DSC++ loss on the DRIVE dataset. Top: Recall, precision and DSC scores at different softmax thresholds for the DSC and DSC++ loss. The vertical bars represent the 95% confidence intervals. Bottom: Example segmentation output at different softmax thresholds. The false positive are highlighted in magenta, and the false negatives are highlighted in green.

recall or precision outputs, such as the Tversky loss modification of the DSC loss [23]. However, after model training, it is not possible to further modify the recall-precision bias, which would instead require the training of a new model. Softmax thresholding is used during post-processing and is therefore independent of the model, enabling flexible and reversible control over the recall-precision bias. Even without softmax thresholding, the uncertainty associated with well calibrated predictions can highlight regions of interest which may be missed when interpreting poorly calibrated predictions (Figure 3).

Given the widespread use of these functions, it is important to consider whether there are any reasons to not replace them with these alternatives. Neither softmax thresholding nor the DSC++ loss has any effect on performance over using the conventional argmax function or DSC loss respectively. Softmax thresholding has no limitations compared to the argmax function, but it is only necessary to use if there is a preference towards recall or precision. The one apparent limitation of using the DSC++ loss over the DSC loss is additional hyperparameter tuning required. However, we investigated a large range of γ values (Table III and Figure 2), and observed that performance was not significantly affected, while the calibration improves significantly, even with small values of γ . Moreover, we selected a γ value of 2 based on results from the DRIVE dataset, and this appeared to generalise well across the other four datasets, with consistently significant improvements to calibration (Table IV). Therefore, even small γ parameter values appear to be effective, and optimal choices for γ generalise well across datasets, suggesting that the γ parameter is relatively easy to optimise.

While it is therefore apparent that the DSC++ loss should be favoured over the DSC loss, it is less clear whether the DSC++ loss

should be favoured above other loss functions. Besides calibration, the DSC++ loss suffers from the same limitations as the DSC loss, namely the unstable gradient, resulting from gradient calculations involving small denominators [10], [38]. While there is currently little empirical evidence relating the unstable gradient to suboptimal performance, it has been suggested that incorporating the CE loss helps to mitigate the unstable gradients generated by the DSC loss [39]. Our experiments confirm previous results that compound loss functions generally perform better [5], [6]. However, even if the DSC++ cannot replace these loss functions, we have shown that replacing the DSC component of loss functions with the DSC++ loss leads to significant improvements in calibration, as well as evidence of better performance (Table V).

In future work, we will investigate the effect of gradient instability on the performance of the DSC++ loss. It would be important to evaluate the performance on highly class imbalanced datasets, where gradient stabilisation may be expected to be more important. Furthermore, it would be useful to evaluate networks trained using the DSC++ loss on out-of-distribution data, to test whether the model predictions remain well calibrated. Finally, the DSC++ loss may be readily extended to 3D and multiclass biomedical image segmentation tasks, and it would be useful to investigate whether the improvement in calibration generalises to these datasets.

V. CONCLUSION

In this study, we identified the main reason behind neural network overconfidence when training deep learning based image segmentation models using the DSC loss, and provided a simple yet effective modification, named the DSC++ loss, that directly addresses the

issue. After evaluating the performance and calibration of both the DSC loss and DSC++ loss across five well-validated biomedical imaging datasets, as well as systematically analysing the softmax predictions, it is clear that the DSC loss is not suitable for training neural networks for use in biomedical or clinical practice. In contrast, the DSC++ loss, together with its synergistic effect using softmax thresholding, produce model outputs that are useful to interpret, and readily adjustable to provide high recall or precision outputs. Compared with previous methods used to improve the calibration of networks trained using the DSC loss, the DSC++ loss provides the most intuitive, readily accessible solution that is an important contribution towards the goal of deploying deep learning image segmentation systems into biomedical or clinical practice.

REFERENCES

- [1] Nikhil R Pal and Sankar K Pal, “A review on image segmentation techniques,” *Pattern Recognit.*, vol. 26, no. 9, pp. 1277–1294, 1993.
- [2] Holger R Roth, Le Lu, Amal Farag, Hoo-Chang Shin, Jiamin Liu, Erim B Turkbey, and Ronald M Summers, “Deeporgan: Multi-level deep convolutional networks for automated pancreas segmentation,” in *International conference on medical image computing and computer-assisted intervention*. Springer, 2015, pp. 556–564.
- [3] Annika Reinke, Matthias Eisemann, Minu D Tizabi, Carole H Sudre, Tim Rädsch, Michela Antonelli, Tal Arbel, Spyridon Bakas, M Jorge Cardoso, Veronika Cheplygina, et al., “Common limitations of image processing metrics: A picture story,” *arXiv preprint arXiv:2104.05642*, 2021.
- [4] Lucas Fidon, Wenqi Li, Luis C Garcia-Peraza-Herrera, Jinendra Ekanayake, Neil Kitchen, Sébastien Ourselin, and Tom Vercauteren, “Generalised wasserstein dice score for imbalanced multi-class segmentation using holistic convolutional networks,” in *International MICCAI Brain lesion Workshop*. Springer, 2017, pp. 64–76.
- [5] Jun Ma, Jianan Chen, Matthew Ng, Rui Huang, Yu Li, Chen Li, Xiaoping Yang, and Anne L Martel, “Loss odyssey in medical image segmentation,” *Med. Image Anal.*, p. 102035, 2021.
- [6] Michael Yeung, Evis Sala, Carola-Bibiane Schönlieb, and Leonardo Rundo, “Unified focal loss: Generalising dice and cross entropy-based losses to handle class imbalanced medical image segmentation,” *arXiv preprint arXiv:2102.04525*, 2021.
- [7] Fausto Milletari, Nassir Navab, and Seyed-Ahmad Ahmadi, “V-Net: Fully convolutional neural networks for volumetric medical image segmentation,” in *Proc. Fourth International Conference on 3D Vision (3DV)*. IEEE, 2016, pp. 565–571.
- [8] Carole H Sudre, Wenqi Li, Tom Vercauteren, Sébastien Ourselin, and M Jorge Cardoso, “Generalised dice overlap as a deep learning loss function for highly unbalanced segmentations,” in *Deep learning in medical image analysis and multimodal learning for clinical decision support*, pp. 240–248. Springer, 2017.
- [9] Tom Eelbode, Jeroen Bertels, Maxim Berman, Dirk Vandermeulen, Frederik Maes, Raf Bisschops, and Matthew B Blaschko, “Optimization for medical image segmentation: theory and practice when evaluating with dice score or jaccard index,” *IEEE Trans. Med. Imaging*, vol. 39, no. 11, pp. 3679–3690, 2020.
- [10] Jeroen Bertels, David Robben, Dirk Vandermeulen, and Paul Suetens, “Optimization with soft dice can lead to a volumetric bias,” in *International MICCAI Brainlesion Workshop*. Springer, 2019, pp. 89–97.
- [11] Alireza Mehrtash, William M Wells, Clare M Tempany, Purang Abolmaesumi, and Tina Kapur, “Confidence calibration and predictive uncertainty estimation for deep medical image segmentation,” *IEEE Trans. Med. Imaging*, vol. 39, no. 12, pp. 3868–3878, 2020.
- [12] Jeroen Bertels, David Robben, Dirk Vandermeulen, and Paul Suetens, “Theoretical analysis and experimental validation of volume bias of soft dice optimized segmentation maps in the context of inherent uncertainty,” *Med. Image Anal.*, vol. 67, pp. 101833, 2021.
- [13] Jörg Sander, Bob D de Vos, Jelmer M Wolterink, and Ivana Išgum, “Towards increased trustworthiness of deep learning segmentation methods on cardiac mri,” in *Medical Imaging 2019: Image Processing*. International Society for Optics and Photonics, 2019, vol. 10949, p. 1094919.
- [14] Axel-Jan Rousseau, Thijs Becker, Jeroen Bertels, Matthew B Blaschko, and Dirk Valkenborg, “Post training uncertainty calibration of deep networks for medical image segmentation,” in *2021 IEEE 18th International Symposium on Biomedical Imaging (ISBI)*. IEEE, 2021, pp. 1052–1056.
- [15] Mohsen Ghafoorian, Alireza Mehrtash, Tina Kapur, Nico Karssemeijer, Elena Marchiori, Mehran Pesteie, Charles RG Guttmann, Frank-Erik de Leeuw, Clare M Tempany, Bram Van Ginneken, et al., “Transfer learning for domain adaptation in mri: Application in brain lesion segmentation,” in *International conference on medical image computing and computer-assisted intervention*. Springer, 2017, pp. 516–524.
- [16] Tsung-Yi Lin, Priya Goyal, Ross Girshick, Kaiming He, and Piotr Dollar, “Focal loss for dense object detection,” in *Proc. International Conference on Computer Vision (ICCV)*. IEEE, Oct 2017, pp. 2999–3007.
- [17] Yafen Dong, Xiaohong Shen, Zhe Jiang, and Haiyan Wang, “Recognition of imbalanced underwater acoustic datasets with exponentially weighted cross-entropy loss,” *Appl. Acoust.*, vol. 174, pp. 107740, 2021.
- [18] Yarin Gal and Zoubin Ghahramani, “Dropout as a bayesian approximation: Representing model uncertainty in deep learning,” in *international conference on machine learning*. PMLR, 2016, pp. 1050–1059.
- [19] John Platt et al., “Probabilistic outputs for support vector machines and comparisons to regularized likelihood methods,” *Advances in large margin classifiers*, vol. 10, no. 3, pp. 61–74, 1999.
- [20] Terrance DeVries and Graham W Taylor, “Leveraging uncertainty estimates for predicting segmentation quality,” *arXiv preprint arXiv:1807.00502*, 2018.
- [21] Balaji Lakshminarayanan, Alexander Pritzel, and Charles Blundell, “Simple and scalable predictive uncertainty estimation using deep ensembles,” *arXiv preprint arXiv:1612.01474*, 2016.
- [22] Tilmann Gneiting and Adrian E Raftery, “Strictly proper scoring rules, prediction, and estimation,” *J Am Stat Assoc*, vol. 102, no. 477, pp. 359–378, 2007.
- [23] Seyed Sadegh Mohseni Salehi, Deniz Erdogmus, and Ali Gholipour, “Tversky loss function for image segmentation using 3D fully convolutional deep networks,” in *Proc. International Workshop on Machine Learning in Medical Imaging*. Springer, 2017, pp. 379–387.
- [24] Chuan Guo, Geoff Pleiss, Yu Sun, and Kilian Q Weinberger, “On calibration of modern neural networks,” in *International Conference on Machine Learning*. PMLR, 2017, pp. 1321–1330.
- [25] Tim Pearce, Alexandra Brintrup, and Jun Zhu, “Understanding softmax confidence and uncertainty,” *arXiv preprint arXiv:2106.04972*, 2021.
- [26] Joes Staal, Michael D Abràmoff, Meindert Niemeijer, Max A Viergever, and Bram Van Ginneken, “Ridge-based vessel segmentation in color images of the retina,” *IEEE Trans. Med. Imaging*, vol. 23, no. 4, pp. 501–509, 2004.
- [27] Moi Hoon Yap, Gerard Pons, Joan Martí, Sergi Ganau, Melcior Sentís, Reyer Zwiggelaar, Adrian K Davison, and Robert Martí, “Automated breast ultrasound lesions detection using convolutional neural networks,” *IEEE J Biomed Health Inform*, vol. 22, no. 4, pp. 1218–1226, 2017.
- [28] Juan C Caicedo, Allen Goodman, Kyle W Karhohs, Beth A Cimini, Jeanelle Ackerman, Marzieh Haghghi, CherKeng Heng, Tim Becker, Minh Doan, Claire McQuin, et al., “Nucleus segmentation across imaging experiments: the 2018 data science bowl,” *Nat. Methods*, vol. 16, no. 12, pp. 1247–1253, 2019.
- [29] Noel Codella, Veronica Rotemberg, Philipp Tschandl, M Emre Celebi, Stephen Dusza, David Gutman, Brian Helba, Aadi Kalloo, Konstantinos Liopyris, Michael Marchetti, et al., “Skin lesion analysis toward melanoma detection 2018: A challenge hosted by the international skin imaging collaboration (isic),” *arXiv preprint arXiv:1902.03368*, 2019.
- [30] Jorge Bernal, F Javier Sánchez, Gloria Fernández-Esparrach, Debora Gil, Cristina Rodríguez, and Fernando Vilariño, “Wm-dova maps for accurate polyp highlighting in colonoscopy: Validation vs. saliency maps from physicians,” *Comput Med Imaging Graph*, vol. 43, pp. 99–111, 2015.
- [31] Dominik Müller and Frank Kramer, “Miscnn: a framework for medical image segmentation with convolutional neural networks and deep learning,” *BMC Med. Imaging*, vol. 21, no. 1, pp. 1–11, 2021.
- [32] Olaf Ronneberger, Philipp Fischer, and Thomas Brox, “U-net: Convolutional networks for biomedical image segmentation,” in *International Conference on Medical image computing and computer-assisted intervention*. Springer, 2015, pp. 234–241.
- [33] Xiao-Yun Zhou and Guang-Zhong Yang, “Normalization in training U-Net for 2-D biomedical semantic segmentation,” *IEEE Robot. Autom. Lett.*, vol. 4, no. 2, pp. 1792–1799, 2019.
- [34] Nabila Abraham and Naimul Mefraz Khan, “A novel focal tversky loss function with improved attention u-net for lesion segmentation,” in *2019 IEEE 16th International Symposium on Biomedical Imaging (ISBI 2019)*. IEEE, 2019, pp. 683–687.

- [35] Saeid Asgari Taghanaki, Yefeng Zheng, S Kevin Zhou, Bogdan Georgescu, Puneet Sharma, Daguang Xu, Dorin Comaniciu, and Ghassan Hamarneh, “Combo loss: Handling input and output imbalance in multi-organ segmentation,” *Comput. Med. Imaging Graph.*, vol. 75, pp. 24–33, 2019.
- [36] Michal Drozdzal, Eugene Vorontsov, Gabriel Chartrand, Samuel Kadoury, and Chris Pal, “The importance of skip connections in biomedical image segmentation,” in *Deep learning and data labeling for medical applications*, pp. 179–187. Springer, 2016.
- [37] Alba Nogueira-Rodríguez, Rubén Domínguez-Carbajales, Hugo López-Fernández, Águeda Iglesias, Joaquín Cubiella, Florentino Fdez-Riverola, Miguel Reboiro-Jato, and Daniel Glez-Peña, “Deep neural networks approaches for detecting and classifying colorectal polyps,” *Neurocomputing*, vol. 423, pp. 721–734, 2021.
- [38] Ken CL Wong, Mehdi Moradi, Hui Tang, and Tanveer Syeda-Mahmood, “3d segmentation with exponential logarithmic loss for highly unbalanced object sizes,” in *International Conference on Medical Image Computing and Computer-Assisted Intervention*. Springer, 2018, pp. 612–619.
- [39] Fabian Isensee, Paul F Jaeger, Simon AA Kohl, Jens Petersen, and Klaus H Maier-Hein, “nnu-net: a self-configuring method for deep learning-based biomedical image segmentation,” *Nat. Methods*, vol. 18, no. 2, pp. 203–211, 2021.